CHAPTER VII

INHIBITION OF MILD STEEL CORROSION IN 1M HYDROCHLORIC ACID USING (E)-(4-(4-METHOXY-BENZYLIDENEAMINO)-4H-1, 2, 4-TRIAZOLE-3, 5-DIYL) DIMETHANOL (MBATD)

The work presented in this chapter is accepted for publication in Journal of dispersion science and Technology.Ms JDST 2012/39.

7.1 MEDIUM

The medium for the study was prepared from reagent grade HCl (E.merk) and double distilled water. All the tests were performed in aerated medium at different temperatures under normal atmospheric pressure.

7.2 INHIBITOR MOLECULE

The inhibitor, (E)-(4-(4-methoxybenzylideneamino)-4H-1, 2, 4-triazole-3, 5-diyl) dimethanol (MBATD) synthesized by procedure given in chapter V, section 5.3. The structure of the water soluble compound is given in Fig 7.1.

7.3 RESULTS AND DISCUSSION

7.3.1. Potentiodynamic Polarization Studies

The potentiodynamic polarization curves obtained in the potential range from –250 mV to +250 mV with a sweep rate of 1 mV/ sec. The numerical values of the variations in corrosion current density (i_{corr}), corrosion potential (E_{corr}), anodic Tafel slope (β_a), cathodic Tafel slope (β_c) and inhibition efficiency (%IE) with various concentrations of inhibitor at different temperatures are summarized in Table Vll.1.It is clear from this Table that that i_{corr} value increase with temperature and decreases with the addition of MBATD. This behavior of the inhibitor molecule can be interpreted based on its adsorption characteristics on the metal surface. The increase in temperature activate the desorption process and some adsorbed inhibitor molecules looses from the metal surface, leading to a decrease in the inhibition efficiency [1].

In acidic solutions, the anodic reaction is the movement of metal ions from the working electrode into the solution, and the cathodic reaction is the discharge of hydrogen ions to hydrogen gas or reducing the concentration of oxygen. The inhibitor may affect either the anodic or the cathodic reaction or both [2]. Since the anodic Tafel slope (β_a) and cathodic Tafel slope (β_c) of MBATD were found to change with inhibitor concentration, the inhibitor affected both of these reactions and act as a mixed-type inhibitor [3]. The polarization profile of mild steel in 1 M hydrochloric acid at 303,313 & 323K in the presence and absence of MBATD is shown in Fig.7.2a, 2b & 2c. The

presence of MBATD led to a decrease in the cathodic and anodic current density at all temperatures under study. The adsorption of inhibitor can affect the corrosion rate in two ways: (i) by decreasing the available reaction area, the so-called geometric blocking effect and (ii) by modifying the activation energy of the cathodic and/or anodic reactions occurring in the inhibitor-free metal in the course of the inhibited corrosion process. It is a difficult task to determine which aspects of the inhibiting effect are connected to the geometric blocking action and which are connected to the energy effect. Theoretically, no shifts in E_{corr} should be observed after addition of the corrosion inhibitor if the geometric blocking effect is stronger than the energy effect [4].The change observed in the E_{corr} values upon addition of MBATD therefore indicates the energy effect is stronger than the blocking effect.

7.3.2 Electrochemical Impedance Spectroscopy

Electrochemical impedance spectroscopy (EIS) measurements were carried out in the frequency range 10 kHz to 0.1 Hz with amplitude of 10 mV (RMS) using a.c signals at open circuit potential. Nyquist, Bode and impedance plots of mild steel in 1M HCl in the absence and presence of MBATD at different temperatures are given in Fig.7.3(a-c),4(a-c) & 5(a-c).The Nyquist diagrams show single capacitive loop, with increasing diameter with concentration of the inhibitor, attributed to charge transfer of the corrosion process. It is evident from Fig.7.3 (a-c) that the impedance loops measured are depressed semi-circles with their centers below the real axis due to the roughness and other in- homogeneities of the electrode surface [5-7]. So one constant phase element (Q) is substituted for the capacitive element in the equation to get a more accurate fit. The impedance of a constant phase element is described by the expression:

$$Z_Q = \mathbf{Y}_0^{-1} (\mathbf{j\omega})^{-\mathbf{n}}$$

where Y_0 is a proportional factor, n has the meaning of a phase shift. For n = 0, Q represents a resistance; for n = 1, a capacitance; for n = 0.5, a Warburg element and for n =-1 an inductance. According to Hsu and Mansfeld [8], the

values of the double layer capacitance (C_{dl}) can be obtained from the equation:

$$C_{dl} = \mathbf{Yo}(\omega''_{\mathbf{m}})^{\mathbf{n}-1}$$

where $\omega''_{\mathbf{m}}$ is the frequency at which the imaginary part of the impedance has a maximum.

Charge transfer resistance (R_{ct}) and double layer capacitance (C_{dl}) were given in TableVll.2. It is observed from Table Vll.2 that the values of the polarization resistance increases with the increase in inhibitor concentration, due to the corrosion protection effect of the inhibitor molecules. The inhibition efficiencies calculated from EIS studies, show the same trend of polarization measurements. The difference of inhibition efficiency of these two methods may be attributed to the different surface status of the electrode in these two measurements. EIS measurements were performed at the rest potential, while in polarization measurements the electrode surface was polarized due to high overpotential, non-uniform current distributions resulted from cell geometry, solution conductivity, counter and reference electrode placement etc. and will lead to the difference between the electrode area actually undergoing polarization and the total area [9]. As it can be seen from Table Vll.2, the C_{dl} values tend to decrease with the increase of the inhibitor concentration. The decrease in the C_{dl}, which can result from a decrease in local dielectric constant and/or an increase in the thickness of the electrical double layer, suggests that MBATD molecule functions by adsorption at the metal/solution interface [10].

7.3.3 Adsorption Isotherm and Thermodynamic Parameters

From attempts to fit the θ values to different isotherms, the best-fit result obtained with the Langmuir isotherm. The plot of (C_{inh}/θ) versus C_{inh} gave straight line graphs at various temperatures are shown in Fig .7.6. The values of linear regression coefficients (R^2) are almost equal to1, confirming that the adsorption of MBATD in 1M HCl solution follow the Langmuir adsorption

isotherm. The free energy of adsorption (ΔG^{o}_{ads}) is related to the adsorption constant (K_{ads}) with following equation [11].

$$K_{ads} = \frac{1}{55.5}\exp(\frac{-\Delta G^{o}_{ads}}{RT}) \quad (1)$$

where R is the universal gas constant, T the thermodynamic temperature and 55.5 is the concentration of water in the solution expressed in mol^{-1}. The values of free energy of adsorption and adsorption constant are listed in Table Vll.3.The negative values of ΔG^{o}_{ads} and the higher values of K_{ads} ($\geq 100M^{-1}$) ensures the spontaneity of the adsorption process and are characteristics of strong interaction and stability of the adsorbed layer with the mild steel surface [12]. It is generally accepted that the values of ΔG^{o}_{ads} up to -20 kJ/mol are consistent with electrostatic interaction between the charged molecules and the charged metal (physisorption), and, the value around -40 kJ/mol or higher are associated with chemisorption because of sharing or transfer of electrons from organic molecules to the metal surface to form a coordinate type of bond [13].The values of calculated ΔG^{o}_{ads} corresponding to MBATD is between -36 $kjmol^{-1}$ and -38 $kjmol^{-1}$.This indicates that the adsorption is not a simple physical adsorption but it may involve some other interactions also. The thermodynamic parameters are also important for studying the mechanism of corrosion inhibition. The heat of adsorption (ΔH^{0}_{ads}) is calculated using the Van't Hoff equation.

$$\ln K_{ads} = \frac{-\Delta H^{0}_{ads}}{RT} + \text{constant} \quad (2)$$

To calculate the heat of adsorption, ln K_{ads} and 1/T was plotted and is given in Fig.7.7. From the straight line graph the slope ($-\Delta H^{0}_{ads}/R$) and intercept ($\Delta S^{0}_{ads}/R+\ln 1/55.5$) values are calculated. The calculated values of heat of adsorption and entropy of adsorption are given in Table Vll.3. The negative sign of ΔH^{0}_{ads} indicates that the adsorption of inhibitor molecule is an exothermic process. The positive value of ΔS^{0}_{ads} in the presence of the

inhibitor suggests that an increase in disordering takes place on going from reactants to the metal adsorbed reaction species [14].

7.3.4 Effect of Temperature and Kinetic Parameters

The effect of temperature on various corrosion parameters E_{corr}, i_{corr} and % IE were studied in 1M HCl at three different temperatures, 303, 313 & 323 K in the absence and presence of different inhibitor concentrations. Variation of temperature has almost no effect on the general shape of the polarization curves. The results were listed in Table Vll.1 & Vll.2. Inspection of above tables shows that, as the temperature increase, the values of i_{corr} increases and inhibition efficiency and surface coverage decreases. This proves that the inhibition occurs through the adsorption of MBATD on mild steel surface.

The inhibition properties of MBATD can be explained by means of kinetic model. The activation parameters were calculated from Arrhenius equation and transition state equations [15-16]:

$$i_{corr}=k\exp\left(-\frac{E_a}{RT}\right) \tag{3}$$

$$i_{corr}=\frac{RT}{Nh}\exp\left(\frac{\Delta S^{\circ}_a}{R}\right)\exp\left(-\frac{\Delta H^{\circ}_a}{RT}\right) \tag{4}$$

where E_a is the activation energy, k is the Arrhenius pre-exponential factor, T is the absolute temperature, R is the gas constant, h is plank's constant, N is Avogadro's number ΔS°_a is the entropy of activation and ΔH^{0}_a is the enthalpy of activation .

A plot of ln i_{corr} versus 1/T gave a straight line as shown in Fig.7.8. The values of activation energy obtained from the slope of the lines are listed in Table Vll.4**.** The increase of E_a value with MBATD may be due to either physical adsorption that occurs in the first stage or due to decrease in the adsorption of the inhibitor molecule on the mild steel surface with increase of temperature [17-19]. To obtain the values of enthalpy and entropy of activation processes a plot of ln (i_{corr}/T) against 1/T is constructed and given in Fig.7.9. Straight lines were obtained with a slope of (-ΔH/R) and an

intercept of [ln (R/Nh) + (ΔS/R)] and the calculated values of ΔH and ΔS are given in Table Vll.4. The positive signs of the enthalpies (ΔH) reflect the endothermic nature of the mild steel dissolution process suggesting that the dissolution of mild steel is slow in the presence of inhibitor [20]. Large and negative values of entropies (ΔS) imply that the activated complex in the rate determining steps represent the association rather than dissociation, meaning that a decrease in disordering takes place on going from reactant to the activated complex [21]. In addition the less negative values of ΔS in the presence of inhibitor created a near equilibrium corrosion system state [22].

7.3.5 Quantum Chemical Calculations

Quantum chemical calculations were performed to study the effect of structural parameters on the inhibition efficiency of MBATD and its adsorption mechanism on iron surface. The optimized structures for the compound MBATD in its ground state is given in Fig.7.10(a).

Frontier orbital theory is useful in predicting the adsorption centers of the inhibitor molecule responsible for the interaction with surface metal atoms. It is reported that excellent corrosion inhibitors are usually those organic compounds, which not only offer electrons to unoccupied molecular orbital of the metal, but also accept free electrons from the metal. From literature it is clear that the higher the HOMO energy of the inhibitor, the greater the tendency in offering electrons to the unoccupied‘d’ orbital of the metal, and higher the corrosion inhibition efficiency. The lower the LUMO energy, the easier the acceptance of electrons by the pi orbitals of MBATD from the metal surface. The decrease in the LUMO-HOMO energy gap increases the efficiency of the inhibitor. The pictorial representations of the HOMO and LUMO of MBATD are presented in Fig.7.10(b) & (c). Quantum chemical parameters listed in Table VII.5 reveal that MBATD has high HOMO and low LUMO with low-energy gap and thus possess higher inhibition efficiency.The number of electrons transferred (ΔN) was also calculated using the quantum chemical method by the following equation:

$$\Delta N = \frac{\chi_{Fe} - \chi_{inh}}{2(\eta_{Fe} + \eta_{inh})} \quad (5)$$

where χ_{Fe} and χ_{inh} denotes the absolute electro negativity of iron and the inhibitor molecule and, η_{Fe} and η_{inh} denotes the absolute hardness of iron and inhibitor molecules respectively. These are also related to electron affinity (A) and ionization potential (I).

$\chi = (I+A)/2$, $\eta = (I-A)/2$. Where A and I related to E_{HOMO} and $E_{LUMO\ as}$

$I = -E_{HOMO}$, $A = -E_{LUMO}$

Using a theoretical χ value of 7 eV/mol according to Pearson's electro negativity scale, and η value of 0 eV/mol for iron, ΔN was calculated. Values of ΔN showed inhibition effect resulted from electron donation. The results are presented in Table Vll.5. It is accepted that if the value of ΔN is less than 3.6, the inhibition efficiency increases with increasing electron-donating ability at the metal surface [23]. Here, MBATD was the donor of electrons, and the mild steel surface was the acceptor of electrons.

7.3.6 Molecular Dynamics Simulations

Molecular dynamics simulation studies were performed for understanding the interaction between MBATD and mild steel surface. Molecular structure of MBATD shows that it is likely to adsorb on the mild steel surface by sharing electron of nitrogen atom, phenyl ring and triazole structure. The periodic boundary conditions were applied to the simulation cell and the whole system was energy optimized, and the possibility of the MBATD adsorption on the mild steel surface was simulated as in Fig .7.10(d). The adsorption energy, the sum of the rigid adsorption energy and deformation energy for the adsorbate component have been calculated. The rigid adsorption energy reports the energy released in kcal/mol, when the unrelaxed adsorbate components adsorbed on the substrate. The deformation energy reports the energy released when the adsorbed adsorbate components are relaxed on the substrate surface. The results of Monte Carlo simulation [24-26] for adsorption of MBATD molecule on Fe (110) plane, the total energy (E_{total}), rigid adsorption energy

($E_{rigid\ adsorption}$),deformation energy ($E_{deformation}$), dEad/dNi (energy of subsrate-adsorbate configurations where one of the substrate is removed) and binding energy ($E_{binding}$) are presented in Table Vll.6. These values also confirm the adsorption of MBATD on iron surface.

7.3.7 Scanning Electron Microscopy

SEM was also employed to gather additional information on the nature of interaction of the inhibitor molecules on the metal surface. The scanning electron micrographs of mild steel specimen before and after exposure in 1M HCl are shown in Fig .7.11(a) & (b).These graphs clearly show that the surface was covered with high-density pits due to exposure of mild steel in hydrochloric acid. The influence of the addition of 200 ppm MBATD on mild steel specimen in 1M HCl is shown in Fig.7.11(c).This micrograph shows evidence for the formation of film on the metal surface. This film may be formed due to the adsorption of inhibitor molecules around the pits formed on the specimens in the early stages of formation (initiation and propagation).

7.4 CONCLUSIONS

- The inhibitor molecule shows fairly good inhibitive efficiency for mild steel in 1M HCl.
- The percentage inhibition efficiency increases with increase in concentration and decreases with exposure time and temperature.
- The adsorption of MBATD on mild steel surface follow Langmuir adsorption isotherm.
- Polarization studies reveal that MBATD act as a mixed type inhibitor.
- Molecular dynamics simulations confirm the adsorption behavior of MBATD on iron surface.
- The relationship between efficiency of inhibition of iron in 1 M HCl and the E_{HOMO}, $E_{LUMO,}$ E_{LUMO}-E_{HOMO} and ΔN of MBATD were calculated by DFT method and have good agreement with the electrochemical results.

7.5 REFERENCES

1. Noor.E.A & Al-Moubaraki.A.H, *Mater. Chem. Phys*.110 (2008) 145.
2. Saliyan Ramesh.V& Adhikari.A.V, *Corros. Sci.*50 (2008) 55.
3. Liu .F.G, Du.M ,Zhang .J & Qiu.M, *Corros. Sci.* 51 (2009) 102
4. de Souza.F.S, (2009) *Corros. Sci.* 51 (2009) 642.
5. Mansfeld.F, *Corrosion* .37 (1981) 301.
6. Mac Cafferty.E, *Corros. Sci.* 39 (1997) 243.
7. Morad.M.S, *Corros. Sci.* 42 (2000) 1313.
8. Hsu.C.H & Mansfeld.F, *Corrosion.* 57 (2001) 747.
9. Kelly.R.G, Scully.J.R, Shoesmith.D.W & Buchheit.R.G. *Electrochemical Techniques in Corrosion Science and Engineering, Marcel Dekker, Inc. New York.* 148 (2002).
10. Lebrini.M, Lagrenee .M, Traisnel.M, Gengembre.L, Vezin & Bentiss. F, *Appl. Surf. Sci.* 253 (2007) 9267.
11. Cano .E, Polo .J.L, La. Iglesia .A & Bastidas. J.M, *Adsorption.* 10 (2004) 219.
12. Lagrenee .M, Mernari.B, Bouanis.M, Traisnel.M & Bentiss.F, *Corros. Sci***.** 44 (2002) 573.
13. Hosseini.M, Mertens.S.F.L & Arshadi.M.R, *Corros.Sci.* 45(2003) 1473.
14. Bouklah.M, Hammouti.B, Lagrenee.M & Bentiss.F, *Corros. Sci.*48 (2006) 2831.
15. Ostovari .A, Hoseinieh .S.M, Peikari .M, Shadizadeh.S & Hashemi. S, *J. Corros. Sci*10 (2009) 1935.
16. del Campo.L, Perez-Saez.R.B, Gonzalez-Fernandez.L & Tello.M.J. *Corros. Sci.* 51 (2009) 707.
17. Larabi.L, Harek.Y, Benali.O & Ghalem .S, *Prog. Org. Coat.* 54 (2005) 256.
18. Larabi.L, Benali .O & Harek .Y, *Mater. Lett.* 61 (2007) 3287.

19. Szauer.T& Brandt.A, *Electrochim. Acta.* 26 (2004) 1253.

20. Guan.N.M, Xueming .L & Fei. L, *Mater. Chem. Phys.* 86 (2004) 59.

21. Abd El-Rehim.S.S, Hassan.H.H & Amin.M.A, *Mater.Chem.Phys.*70 (2001) 64.

22. Musa.A.Y, Kadhum.A.A.H, Mohamad.A.B, daud.A.R, Takriff.M.S, & Kamarudin.S.K, *corros sci.* 51 (2009) 2393.

23. Lukovits.I,Kalman .E & Zucchi .F, *Corrosion.* 57 **(**2001) 3.

24. Zhao.P, Liang .Q & Li .Y, *Appl.Surf. Sci.* 252 (2005) 1596.

25. Khaled.K.F, *J. of solid state electrochemistry* 13 (2009) 1743.

26. Khaled.K.F, *Corros. Sci*. 52 (2010) 3225

Table Vll.1 Polarization parameters for mild steel in 1M HCl with different concentrations of MBATD at different temperatures.

Temp. (K)	Conc. (ppm)	E_{corr} (mV/SCE)	β_a (mV/dec)	β_c (mV/dec)	i_{corr} ($\mu A/cm^2$)	I.E (%)
303	Blank	-511	70	93	941	---
	10	-509	73	69	389	59
	50	-534	93	87	351	63
	100	-555	70	57	310	67
	200	-544	61	43	192	80
313	Blank	-526	95	114	1894	---
	10	-538	78	110	837	56
	50	-533	67	80	728	62
	100	-541	73	61	632	66
	200	-543	67	72	428	77
323	Blank	-457	93	137	2973	---
	10	-467	97	141	1465	51
	50	-478	75	83	1327	53
	100	-469	90	116	1007	66
	200	-473	83	112	722	75

Table Vll.2 Electrochemical impedance parameters for mild steel in 1 M HCl with different concentrations of MBATD at various temperatures.

Temp. (K)	Conc. (ppm)	R_{ct} (Ω cm^2)	C_{dl} ($\mu F/ cm^2$)	i_{corr} ($\mu A/cm^2$)	C.R (mm/yr)	I.E (%)
303	Blank	329	74	794	0.9201	---
	10	834	55	313	0.3624	61
	50	927	59	282	0.3262	64
	100	1051	50	248	0.2877	69
	200	1802	40	146	0.1680	82
313	Blank	117	142	2222	2.5750	---
	10	270	105	967	1.1211	56
	50	310	87	842	0.9756	62
	100	349	84	747	0.8653	66
	200	561	53	465	0.5391	79
323	Blank	66	225	4084	4.7330	---
	10	139	101	1873	2.1701	52
	50	162	114	1614	1.8713	59
	100	197	93	1327	1.5384	66
	200	298	73	852	0.9874	78

Table Vll.3Thermodynamic parameters for the adsorption of MBATD in 1M HCl on the mild steel in presence of 50 ppm at different temperatures.

Temperature (K)	K_{ads} ($M^{-1}x10^{-4}$)	ΔG^0_{ads} ($kjmol^{-1}$)	ΔH^0_{ads} ($kjmol^{-1}$)	ΔS^0_{ads} ($jmol^{-1}K^{-1}$)
303	4.10	-36.88		
313	3.34	-37.56	-14.66	73.30
323	2.84	-38.32		

Table Vll.4 Activation parameters for mild steel in 1 M HCl in absence and presence of MBATD.

Conc. (ppm)	E_a ($kjmol^{-1}$)	ΔH ($kjmol^{-1}$)	ΔS ($jmol^{-1}K^{-1}$)
Blank	45.64	43.11	-45.57
50	52.62	50.14	-30.76

Table Vll.5 Quantum chemical descriptors for MBATD.

Molecule	E_{HOMO}(eV)	E_{LUMO}(eV)	χ (eV/mol)	η (eV/mol)	ΔN
MBATD	-2.1056	-6.7365	4.4211	2.3155	0.5568

Table Vll.6 Various quantum chemical parameters calculated by simulation studies.

Molecule	E_{total} (kcal/mol)	$E_{adsorption}$ (kcal/mol)	$E_{rigid\ adsorption}$ (kcal/mol)	$E_{deformatio}$ (kcal/mol)	dE_{ad}/dNi (kcal/mol)	$E_{binding}$ kcal/mol)
MBATD	334657.7	295832.9	41386.5	254446.4	295832.9	295833.6

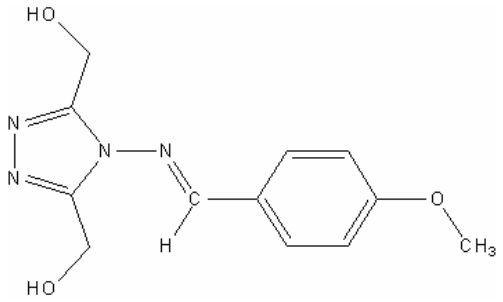

Fig.7.1 Structure of the inhibitor molecule (MBATD).

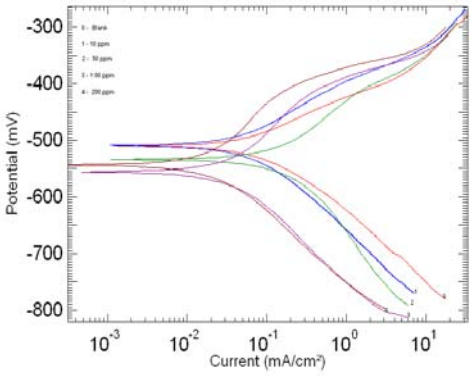

Fig.7.2a

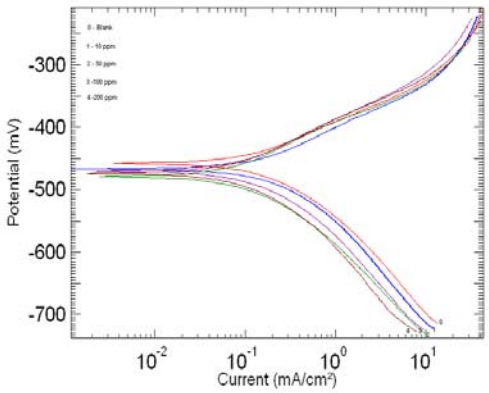

Fig.7.2b

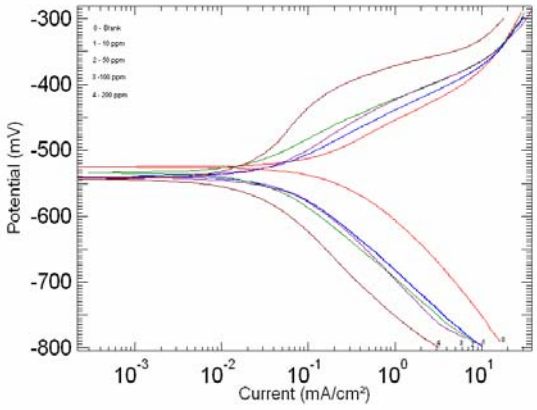

Fig 7.2c

Fig.7.2 Polarization curve of mild steel in 1M HCl in the absence and presence of different concentrations of MBATD at (a) 303 K, (b) 313K & (c) 323K.

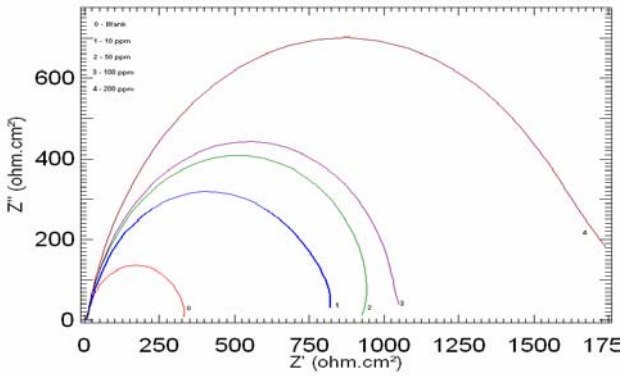

Fig.7.3a

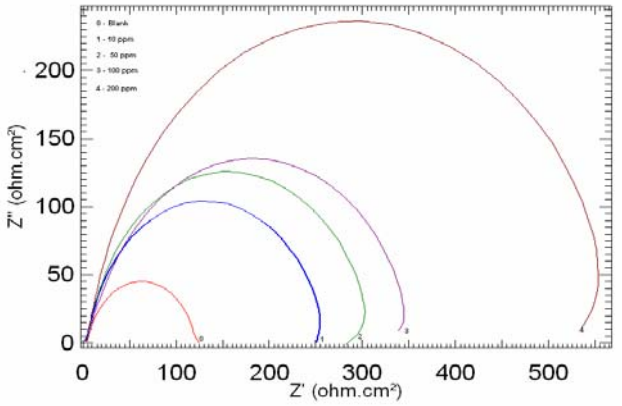

Fig.7. 3b

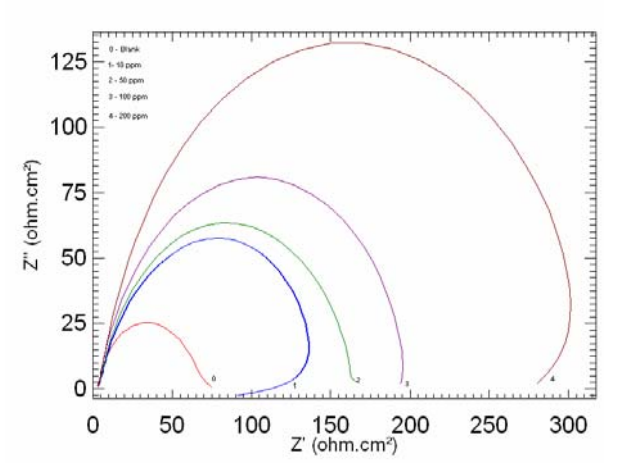

Fig.7. 3c

Fig.7.3 Nyquist plots of mild steel in 1 M HCl in the absence and presence of different concentrations of MBATD at (a) 303, (b) 313 & (c) 323K.

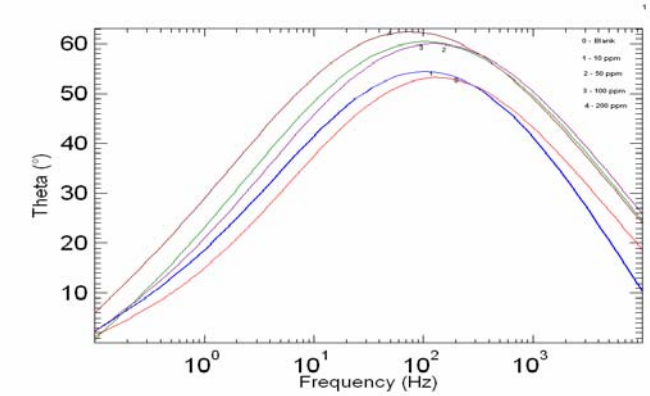

Fig.7.4a

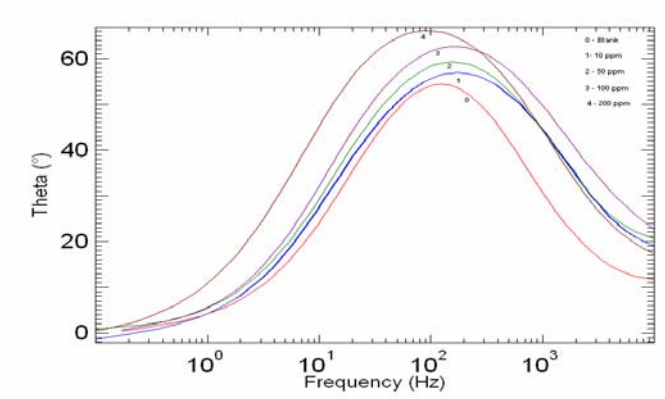

Fig.7. 4b

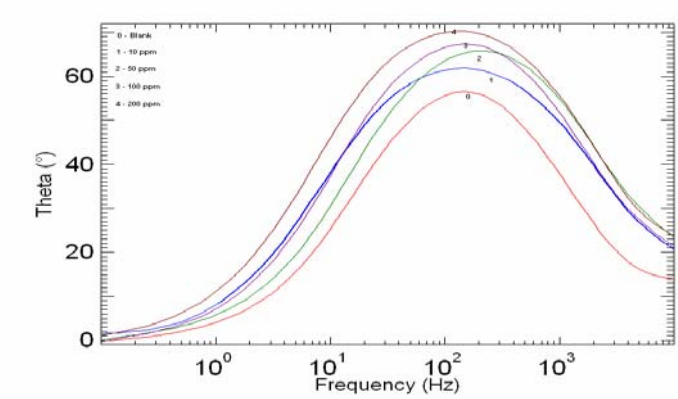

Fig .7.4c

Fig.7.4 Bode plots of mild steel in 1 M HCl in the absence and presence of different concentrations of MBATD at (a) 303,(b)313 & (c) 323K.

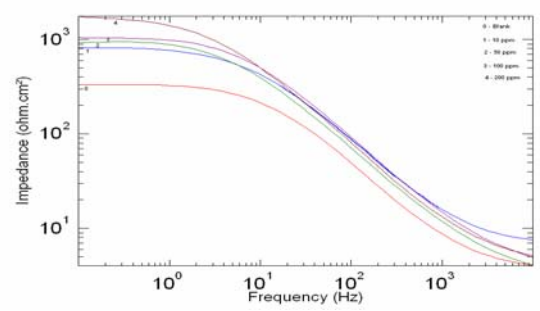

Fig. 7.5a

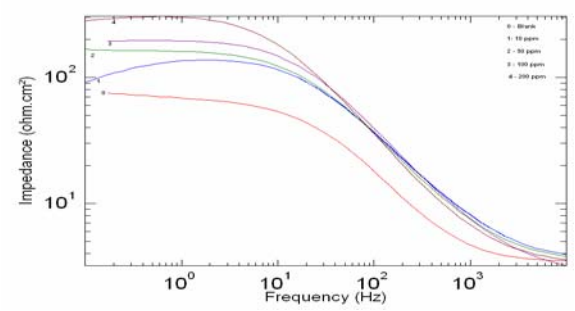

Fig .7.5b

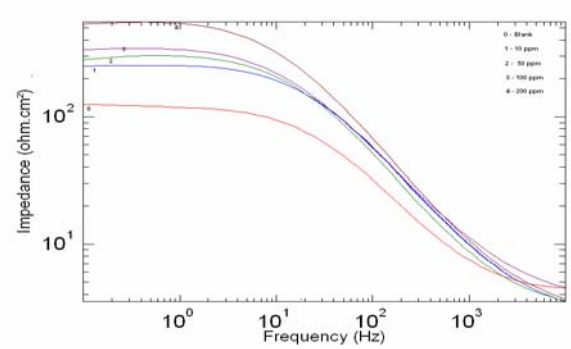

Fig .7.5c

Fig.7.5 Impedance plots of mild steel in 1 M HCl in the absence and presence of different concentrations of MBATD at (a) 303, (b) 313 & (c) 323K.

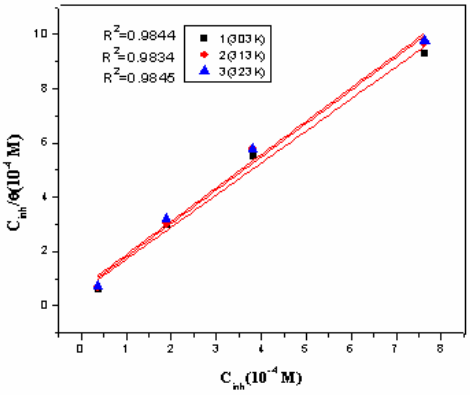

Fig.7.6 Langmuir adsorption isotherm for MBATD on mild steel surface in 1 M HCl (a) 303K(b) 313K and (c) 323K.

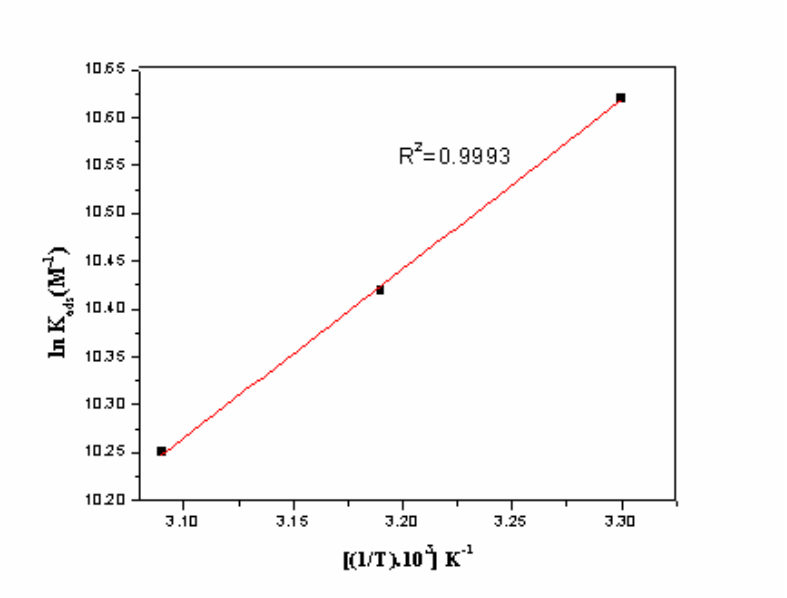

Fig.7.7 Adsorption isotherm plot for ln k_{ads} vs. 1/T of MBATD on mild steel in 1 M HCl.

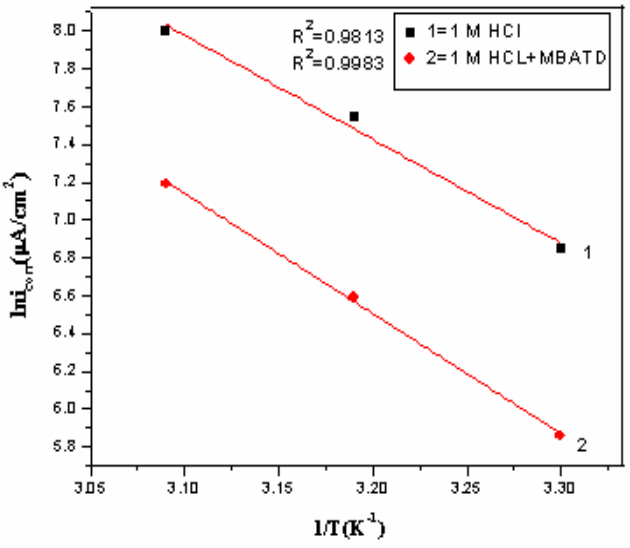

Fig.7.8 Arrhenius plots of ln(i_{corr}) versus 1/T (1) 1M HCl (2) 1M HCl+MBATD.

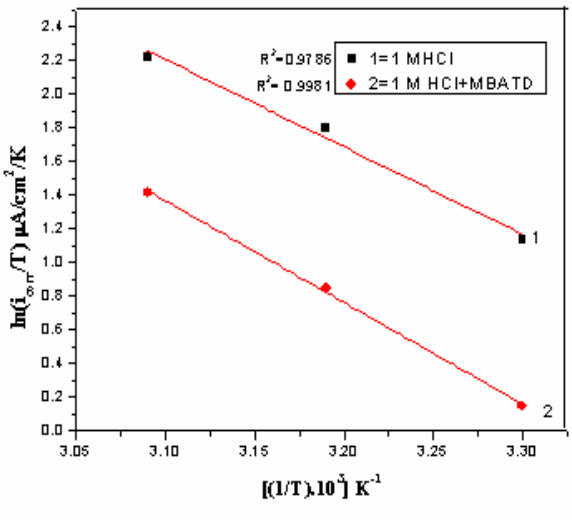

Fig.7.9 Arrhenius plots of $\ln(i_{corr}/T)$ versus 1/T. (1) 1M HCl (2) 1M HCl+MBATD.

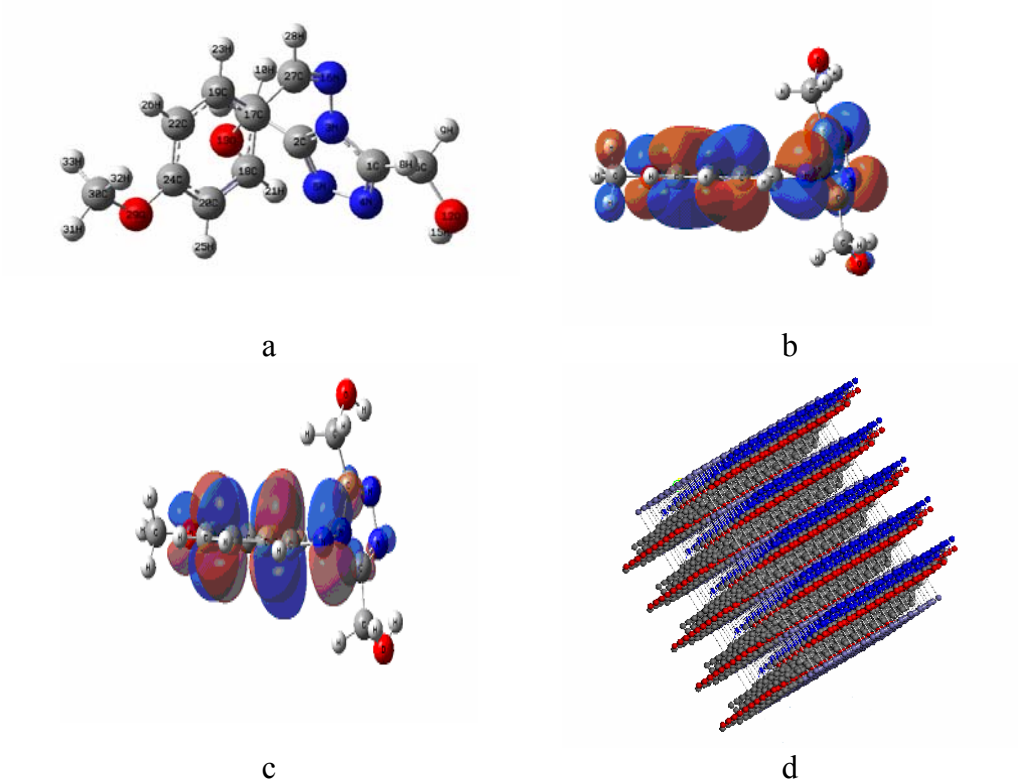

a b

c d

Fig.7.10(a) Optimized geometry of the inhibitor molecule, (b) The highest occupied molecular orbital (HOMO) of the inhibitor, (c) The lowest unoccupied molecular orbital (LUMO) of the inhibitor and (d) Mode of adsorption of inhibitor molecule on iron (110) plane.

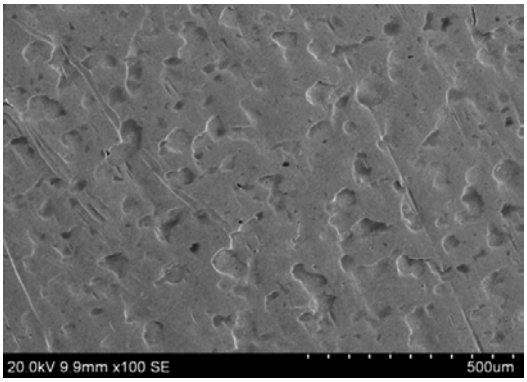

Fig.7.11a

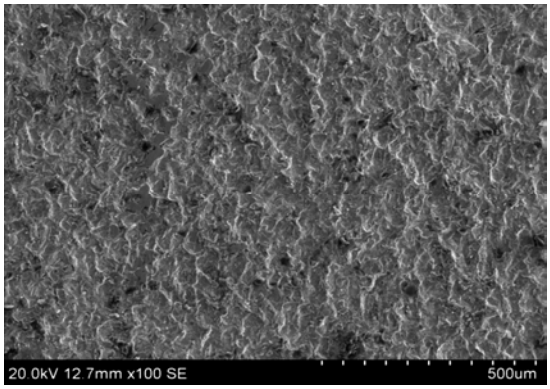

Fig.7.11 b

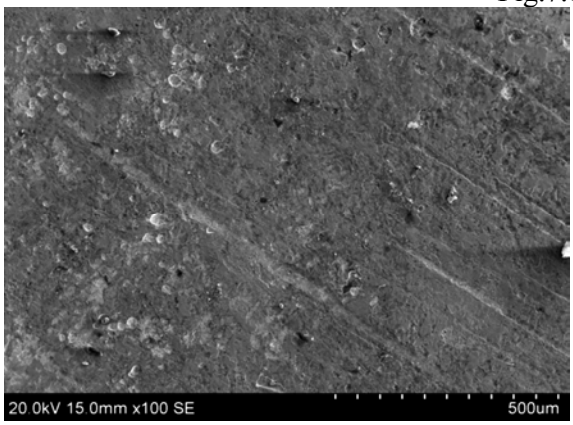

Fig.7.11 c

Fig.7.11 SEM micrographs of 7.11(a) the mild steel before immersion in 1 M HCl, 7.11(b) after immerssion in 1 M HCl and 7.11(c) after immerssion in 1 M HCl containing inhibitor molecule.